Contents

Friday 24$^{\text{th}}$ November, 2017 14:50   [DRAFT v0.1]

INTRODUCTION

Petals are the local support structures holding the ATLAS end-cap ITk strip sensors [1]. For the petal sensors, a series of tests are being designed to cover both Quality Assurance (QA) and Quality Control (QC). These include a series of tests on their assembled structure (through metrology surveys), their electrical functionality and their thermomechanical properties (including ASIC burn in, thermal cycling and long term cold tests). As it's very important that, during the QC process, good care is taken not to damage the fragile components of the sensors, the thermal tests will be made by using infrared thermography, which is the most suitable technique to employ for this purposes. However, depending on the target surface, infrared measurements can be quite inaccurate and unreliable. Silicon, for example, is a tricky material to perform infrared measures on, and it's however the most important component on the detector sensors. That is why a good understanding of infrared thermography is crucial to achieve accurate temperature measurements. For simulating the sensor's response at different operational parameters, thermal Finite Element Analyses (FEAs) are used. In particular, for the petal FEA models, exact design specifications of each component are considered. However, this simulation model have to be validated. For that purpose, numerous building institutes assembled and measured thermo-mechanical module prototypes. In this study, we use the thermomechanical petal prototype assembled at DESY aiming at two main objectives: to contribute to the improvement of the QC and QA processes of the petal structures for the ATLAS end-caps and to perform infrared tests on the current petal thermomechanical prototype in order to provide the FEA team with a comparison point to validate their model. In order to do so, a reliable IR temperature determination is indispensable. To that end, a series of studies were performed to gain better understanding of the way in which those factors affect such measurements:

1. Apparent reflected temperature determination.

2. IR camera's intrinsic spectral response scale factor determination.

3. Emissivity correction/estimation methods for the silicon sensors.

4. Viewing angle influence.

This report contains the results of these studies and is structured as follows: In Chapter 1 a brief background on infrared thermography, needed for the subsequent sections is given. In Chapter 2 a detailed description of the experimental setup used in this work is presented. In Chapter 3, the analysis methods used in the different studies is discussed. Finally, in Chapter 4, the results are presented accompanied by a small discussion.

Chapter 1

Notions of infrared thermography

1.1 Infrared Thermography. Infrared radiation spectrum.

Infrared thermography (IRT) is a science dedicated to the acquisition and processing of thermal information from non-contact measurement devices. Infrared measuring devices acquire infrared radiation emitted by an object and transform it into an electronic signal. As a non-contact technique, IRT has some advantages in relation to other techniques for temperature measurement. For example, the temperature of extremely hot objects or dangerous products, such as acids, can be measured safely, keeping the user out of danger. It also provides protection for the object under investigation since there is no need to attach any temperature measuring device to it which makes it much less invasive. However, there is a caveat: infrared radiation has to reach the IR sensor first, going through some media that can either let it pass almost completely or strongly attenuate it (unless vacuum is used).

Infrared (IR) radiation is the energy irradiated by a surface that has a temperature above the absolute zero [2]. Within the electromagnetic spectrum, IR radiation is defined as the radiation band that spans from 0.7 μm to 1000 μm in wavelength (Figure 1.1). Much of the IR spectrum, however, is generally avoided for IRT applications due to atmospheric absorption. This absorption occurs mainly with H_2O and CO_2 molecules as they are well known for being good heat absorbers (Figure 1.2). According to this fact, the IR wavelength range is sometimes further divided into 4 additional categories:

I. Near-infrared (NIR) from 0.8 μm to 1.7 μm.

II. Short-wavelength infrared (SWIR) from 1 μm to 2.5 μm.

III. Mid-wavelength infrared (MWIR) from 2 μmm to 5 μmm.

IV. Long-wavelength infrared (LWIR) from 8 μmm to 14 μmm.

It is important to note that this classification is somewhat arbitrary and therefore can vary within literature. Most IR sensors are designed to work in the LWIR part of the spectrum since this is the range that minimizes these absorptions.

In this study, as we use an IR camera sensitive only to the fourth type, we will refer to IR as the LWIR except otherwise explicitly stated.

1.2 Plank's law for blackbodies. IR radiation dissipation.

According to Planck's law, the IR emissive power (N) of a blackbody[1] at a temperature T, with a wavelength between λ and $\lambda + d\lambda$ is given by Equation 1.1, where C_1 and C_2 are constant, often called first and second radiation constants respectively [3].

$$N_b(\lambda, T)d\lambda = \frac{C_1 \cdot \lambda^{-5}}{\exp(\frac{C_2}{\lambda \cdot T}) - 1}d\lambda \tag{1.1}$$

---

[1]A blackbody is an idealized physical body that absorbs all incident electromagnetic radiation, regardless of frequency or angle of incidence.
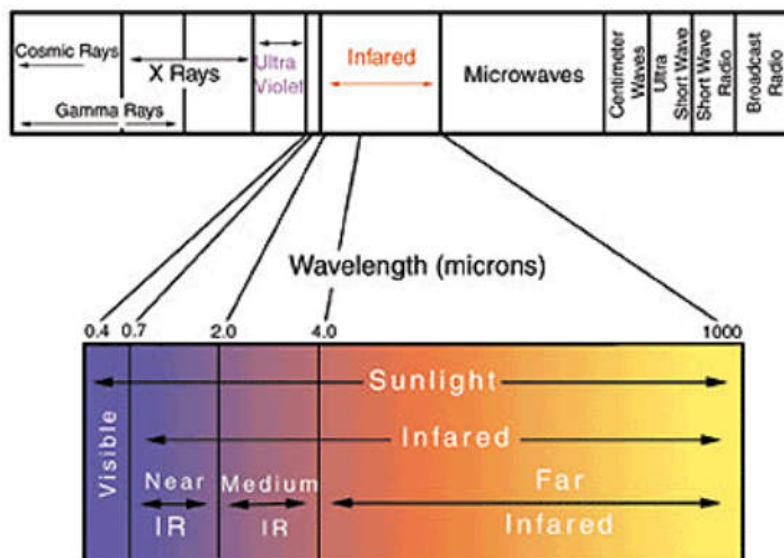
Figure 1.1: Electromagnetic spectrum showing the portion corresponding to
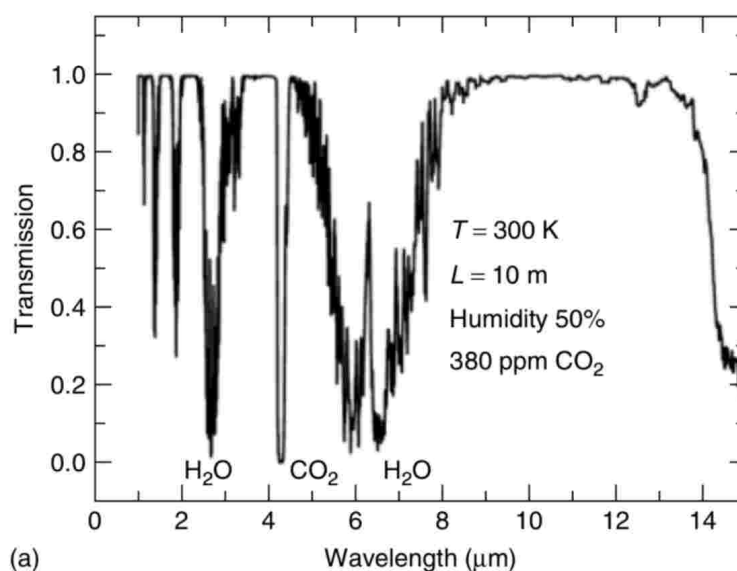IR radiation.

Figure 1.2: An example of atmospheric transmission plot for infrared
radiation. For some of the minima we can see the absorbing molecule
responsible.

Here the subindex b denotes the special case of the blackbody. Figure 1.3 shows this functional dependence in terms of an equivalent magnitude (monochromatic[2] irradiance) for six different temperatures [4]. The gray line represents the displacement of the maximum for each temperature. Note that, as the temperature decreases, the maximum emissive power moves to higher wavelengths, this is known as the Wien's displacement law [5].

There are three ways by which the incoming emissive power may be dissipated: absorption, transmission and reflection [6]. The fractions of the total radiant energy that are associated with each of these modes of dissipation are referred to as the *absorptivity*, *transmissivity* and *reflectivity* of the body. Three parameters are used to describe these phenomena: the spectral absorptance α, which is the fraction of the spectral emissive power absorbed by the object, the spectral reflectance ρ, which is the fraction of the spectral emissive power reflected by the object, and the spectral transmittance τ, which is the fraction

---

[2]Monochromatic here refers to "per wavelength interval". Also referred to as "spectral".

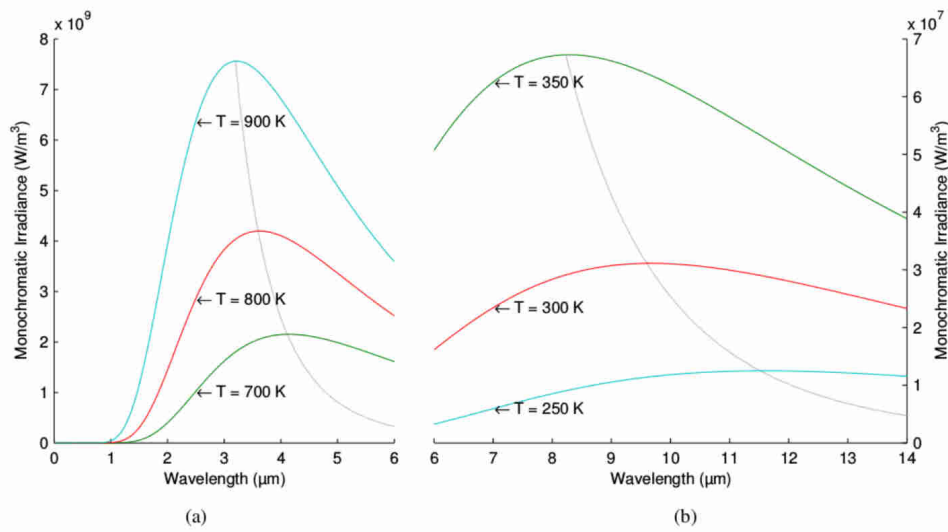of the spectral emissive power transmitted by the object.

Figure 1.3: Planck's law in terms of the monochromatic irradiance of a
blackbody in thermal equilibrium at a definite temperature. (a) Objects with
a high temperature emit most of the radiation in the middle wave infrared;
(b) Objects with a low temperature emit most of the radiation in the long
wave infrared. The two parts of the graph are scaled differently on the y-axis.

These three parameters are, in general, wavelength dependent and their sum must be one at any given
wavelength and surface temperature:

$$\alpha + \rho + \tau = 1 \tag{1.2}$$

If we regard the surface as *opaque*, it means that the transmission coefficient is $\tau \equiv 0$ and then we
can rewrite Equation 1.2 as:

$$\alpha + \rho + \tau = 1 \tag{1.3}$$

In the following we will consider all surfaces as opaque for the derivation of the necessary formulae.
Considering transmission, in those cases where it is absolutely necessary, is a limiting factor since it is
a difficult magnitude to estimate and the additional uncertainties that it would introduced make any
accurate quantitative IR analysis very difficult.

1.3 Emissivity definition. Kirchhoff's law.

One of the most important concepts in IRT is *emissivity* (ε). Emissivity of a surface at a temperature T
for a given wavelength λ is defined as the ratio of the emissive power of a non-blackbody to the emissive
power of a blackbody at the same temperature:

$$\varepsilon(\lambda, T) = \frac{N(\lambda, T)}{N_b(\lambda, T)} \tag{1.4}$$

Here $N(\lambda, T)$ is the emissive power of the non-black body object. As the emissivity of a real surface
typically ranges between 0 and 1, this relationship tells us that real body emits only a fraction of the
thermal energy emitted by a blackbody at the same temperature (Figure 1.4). If the emissivity is constant
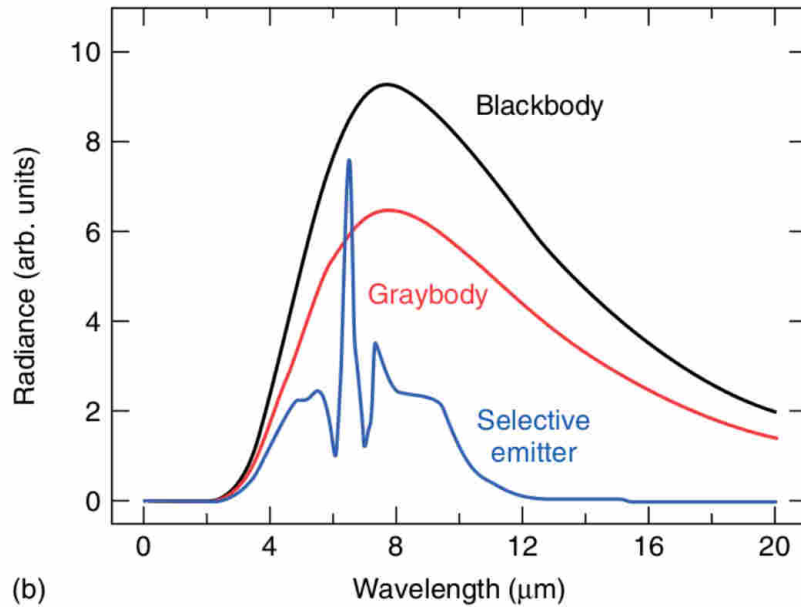and independent of the wavelength, the body is called a *grey body*.

Figure 1.4: Relationship between the blackbody spectral radiation, the
radiation emitted by a grey body and a selective radiator at the same
temperature. It can be seen how the blackbody yields the maximum radiance
at any given wavelength.

The emissivity of real objects, however, varies with respect to wavelength and therefore they cannot be considered grey bodies. In fact, it might also depend on many other factors such as temperature and viewing angle, as we will discuss later. However, it is usually assumed that for short wavelength intervals, the emissivity can be considered constant. This assumption is used to treat real objects as grey bodies in order to avoid the associated mathematical complications of emissivity estimation. For this reason, surface emissivities are often computed as the average of the emissivity through the wavelength interval in which the infrared sensor works. This average is also possible because the emissivity is a slow-varying function of wavelength for solid objects. However, this does not apply to other cases, such as gases or liquids.

A good illustration of the effect of emissivity in the measurement of the real temperature of a surface is presented in Figure 1.5. This corresponds to the so called Leslie's Cube. Even though this cube is filled with hot water and all the faces are at the same temperature we can see a huge difference in the temperature measured by the IR sensor. This is due to the difference in emissivity of the two front faces. One is painted with a high emissivity black (could be any color) paint and therefore the apparent temperature is closer to the real temperature of the water, while the other face has low emissivity (very reflective) and the apparent temperature is almost entirely due to the reflected component (see the heat from the hand reflected in the surface).

The blackbody, as a perfect emitter, will have an emissivity of 1 while non-blackbodies will have, as mentioned earlier, emissivity values in the range $0 < \varepsilon < 1$. If a blackbody is surrounded by an isothermal black enclosure of the same temperature, then, in thermodynamic equilibrium, such blackbody will have to absorb 100% of the radiation emitted by the enclosure. At the same time it will emit 100% of its own thermal radiation since it has $\varepsilon = 1$. Under those circumstances, the following relationship holds:

$$\alpha \equiv \varepsilon = 1 \qquad (1.5)$$

This is known as the Kirchhoff's law (for the blackbody). This law also applies to non-blackbodies and basically tells us that the emissivity and absorptivity of any material are equal at any specified temperature and wavelength. Thus, we can rewrite Equation 1.2 as:

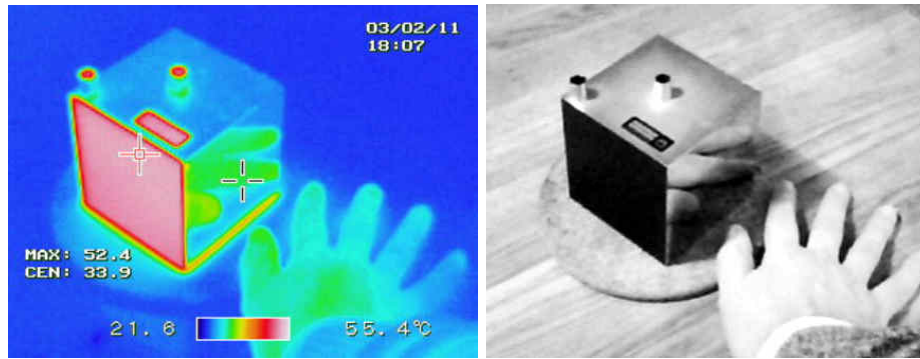$$\varepsilon + \rho + \tau = 1 \qquad (1.6)$$

Figure 1.5: Infrared (Left) and visible (Right) images of a Leslie's cube. The cube is filled with hot water and all the faces are at the same temperature. However, one of the faces is coated with a high emissivity paint (black) and the other has been polished (low emissivity).

And for the case in which transmissivity $\tau = 0$, this becomes:

$$\varepsilon = 1 - \rho \tag{1.7}$$

1.4 IR measurements calibration.

Usually, when we take an IR picture of an object, at room temperature for instance, we intuitively expect the entire image to be of only one color (corresponding to the ambient temperature). However, this is rarely the case. It is important to point out the fact that the IR sensor/camera does not gives us the "real" temperature values but rather an "apparent" one. We refer to these temperatures as *apparent temperatures* since it's necessary later on to correct them due to the presence of several factors that provoque deviations in what the IR sensor perceives. The most important of this factors are:

1. Different emissivity values of the objects in the image.

2. Reflectivity and Transmissivity of the object.

3. Spectral Response Function of the IR camera in the wavelength range in which it operates.

4. Ambient conditions. Apparent reflected temperature.

5. Viewing angle of the IR camera with respect to the object.

6. Surface properties (polishing).

To understand how all this factors come into play we can consider the situation depicted in Figure 1.6. Let's assume that we have a target which is placed in front of a generic IR sensor. We are interested in measuring the amount of radiation coming from the target due to emission alone, since this corresponds to the only measure of the "real" temperature of our object. Using Equation 1.4 we can estimate the amount of emitted IR radiation (N) as:

$$N(\lambda, T) = \varepsilon(\lambda, T) \cdot N_b(\lambda, T) \tag{1.8}$$

Here T is the actual (real) temperature of the target.

In addition, we will have two more contributions to the amount of IR radiation flying in the direction of the sensor. This other contributions are produced by additional sources of heat. The first is the amount
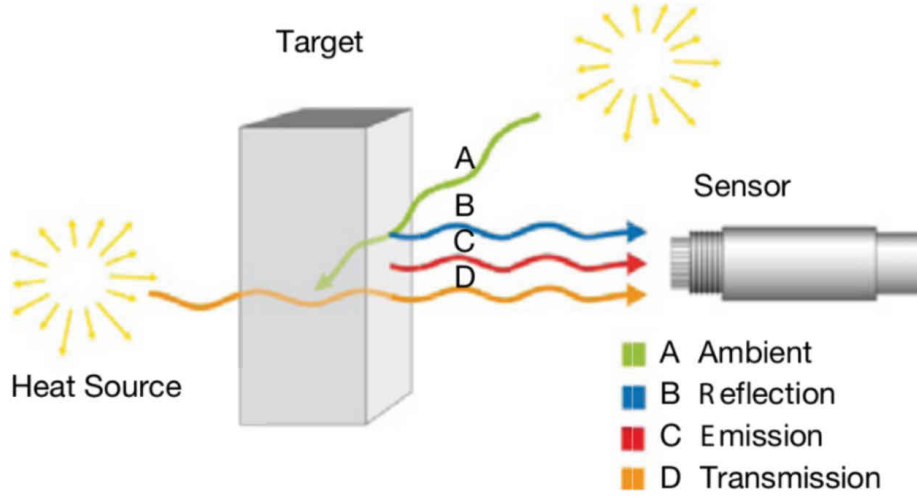
Figure 1.6: Schematics of the IR radiation interaction with a target surface: (A) radiation from an external source being partially absorbed by the target, (B) part of the radiation from A which is is reflected in the direction of the IR camera, (C) thermal radiation emitted from the target and (D) external source radiation transmitted through the target.

of radiation coming from external heat sources that is reflected in the target surface. This contribution is given by:

$$N_{ref}(\lambda, T) = \rho(\lambda, T) \cdot N_b(\lambda, T_r) \tag{1.9}$$

Where T_r is the *apparent reflected temperature* of the target surface. This is an irreducible source of IR background, even with an isolated thermal chamber, and is therefore always present in the estimation of the real surface temperature. In this sense, we can regard the interior walls of the isolation chamber (and all other equipment inside) as "external" heat sources and, as the temperature of such objects should be close to the room temperature, this apparent reflected temperature is often taken as the ambient temperature. We will discuss further on this temperature and its estimation method in Section 3.1. The second source of additional IR radiation is that part of the radiation coming from a heat source behind the target that is transmitted through the target itself. This contribution is determined as:

$$N_{trans}(\lambda, T) = \tau(\lambda, T) \cdot N_b(\lambda, T_t) \tag{1.10}$$

Where T_t is the *apparent transmitted temperature*. This source of IR background can be avoided by placing the target in a thermal enclosure (chamber), leaving all external heat sources outside. However, for complex objects (as the Petal) composed by layers of different materials, this factor can appear if, for example, the surface material (facing the IR sensor) is somewhat transmissive and the heat from other layers reaches them and passes through.

The combination of all these three factors is then the total amount of IR radiation coming from the target that heads towards the camera. Neglecting the transmission component (assuming the object opaque), this amount is:

$$N_{total}(\lambda, T) = N(\lambda, T) + N_{ref}(\lambda, T_r) + N_{trans}(\lambda, T_t) = \varepsilon(\lambda, T) \cdot N_b(\lambda, T) + [1 - \varepsilon(\lambda, T)] \cdot N_b(\lambda, T) \tag{1.11}$$

Where we have used Equation 1.7 to express everything in terms of emissivity. If we also consider that this $N_{total}(\lambda, T)$ is not attenuated in the air path to the IR sensor[3] then the emissive power at temperature T registered by the sensor for a given wavelength is:

$$N_{meas}(\lambda, T) = R(\lambda) \cdot N_{total}(\lambda, T) \tag{1.12}$$

Where $R(\lambda)$ is a correction scale factor introduced to account for the fact that our IR camera is sensitive only in the spectral range from 7.5 μm to 14 μm, and even in that range it's also not 100% sensitive to the incoming radiation. It is often called sensor's *Spectral Response Function* or sensor's *Filter Function*. Note that this factor only depends on the IR sensor's "efficiency" for a given wavelength and it can be estimated as the ratio of the power registered by the sensor and the power calculated using Equation 1.12.

To obtain then the total (integrated over all wavelengths) signal processed by the IR sensor we have to integrate Equation 1.12 over the wavelength range that our sensor is sensitive to (from λ_1=7.5 μm to λ_2=14 μm):

$$N_{meas}(T) = \int_{\lambda_1}^{\lambda_2} N_{meas}(\lambda, T)d\lambda = \int_{\lambda_1}^{\lambda_2} R(\lambda) \cdot N_{total}(\lambda, T)d\lambda \tag{1.13}$$

$$N_{meas}(T) = \int_{\lambda_1}^{\lambda_2} R(\lambda) \cdot \varepsilon(\lambda, T) \cdot N_b(\lambda, T)d\lambda + \int_{\lambda_1}^{\lambda_2} R(\lambda) \cdot [1 - \varepsilon(\lambda, T)] \cdot N_b(\lambda, T_r)d\lambda \tag{1.14}$$

As we don't know the functional form of $R(\lambda)$ or $\varepsilon(\lambda, T)$ with respect to λ we can come around this by applying the integral mean value theorem and use their averaged value instead. Since both $R(\lambda)$ and $\varepsilon(\lambda, T)$ should be slow-varying functions of the wavelength, there must be certain value $\xi \in [\lambda_1, \lambda_2]$ such that we can then express Equation 1.14 as:

$$N_{meas}(T) = R(\xi) \cdot \varepsilon(\xi, T) \cdot \int_{\lambda_1}^{\lambda_2} N_b(\lambda, T)d\lambda + R(\xi) \cdot [1 - \varepsilon(\xi, T)] \cdot \int_{\lambda_1}^{\lambda_2} N_b(\lambda, T_r)d\lambda \tag{1.15}$$

$$N_{meas}(T) = R \cdot \bar{\varepsilon} \cdot I_1(T) + R \cdot [1 - \bar{\varepsilon}] \cdot I_2(T_r) \tag{1.16}$$

Where $\bar{\varepsilon} = \varepsilon(\xi, T)$ is the averaged emissivity in the wavelength region in which the IR camera is most sensitive and $I_1(T)$ and $I_2(T)$ can be calculated numerically:

$$I_1(T) = \int_{\lambda_1}^{\lambda_2} N_b(\lambda, T)d\lambda \tag{1.17}$$

$$I_2(T) = \int_{\lambda_1}^{\lambda_2} N_b(\lambda, T_r)d\lambda \tag{1.18}$$

$R(\xi)$ can also be treated as a constant scale factor (R) which only depends on the IR sensor. One of the studies we performed consisted in taking measurements of this factor using an aluminum bucket filled with water at different temperatures and coated with high emissivity electric tape, obtaining consistent values (See results in Section 4.4). Even though we can assume emissivity as a constant that only depends on the specific material of the surface under investigation, in general, it also depends on the viewing angle of the camera with respect to the normal of the surface. blackbodies behave like perfect isotropically diffuse emitters, that is, for any surface emitting radiation, the radiance of the emitted radiation is independent of the direction into which it is emitted [7]. However, real surfaces, in addition to the lower emission rate (given by lower emissivity) also show angular dependence in the emissive power (Figure 1.7 left).

---

[3]We can see from Figure 1.2 (for 10 m) that the air transmissivity is nearly 1 in the LWIR region of the IR spectrum. Additionally, as our experimental setup was maintained at low humidity, this would further improve the transmissivity of the environment.
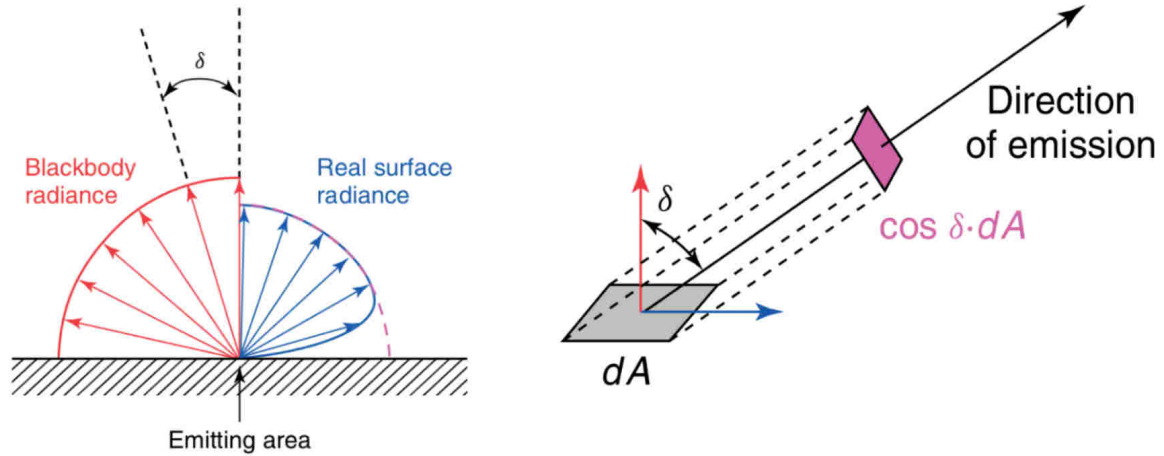
Figure 1.7: Schematics of the angular dependence of the emissive power of a
surface in relation to the blackbody.

Depending on the surface, the intensity of the emitted radiation can be approximated with a cosine
law with good approximation. However, in general, this is not the case, and in most cases a study must
be carried out to estimate the angular dependence of the emissivity.

Chapter 2

Experimental setup

2.1   Thermo Mechanical Petal

Petals are the main component of the two ATLAS end-cap strip detectors which are composed of 6 discs, each with 32 petals (Figure 2.1 left). The petal structure is the frame where the end-cap sensors are mounted. It provides the mechanical and electronic structural support and also contains a titanium alloy cooling pipe for evaporative CO_2 cooling. Each petal holds 6 (silicon) sensors (Figure 2.1 right). For the Phase-II ATLAS upgrade new Petal design is still under development. However, in this study a manually assembled thermomechanical prototype is used, equipped with dummy electronics parts, blank silicon wafers and mechanical components to be a thermal equivalent to the final structure. As the petal's design is still being improved, our prototype became quickly "obsolete". In fact, some key materials for IR studies in the current prototype such as the silicon wafers are not very IR friendly because of their high transmissivity. This makes really difficult the employment of noncontact temperature measuring methods (See Chapter 3). In contrast, newer silicon wafers are available which are not transmissive due to a metallic finish in one of their sides. In that cases, even though the emissivity of silicon is still hard to estimate, more robust IR studies can be performed.
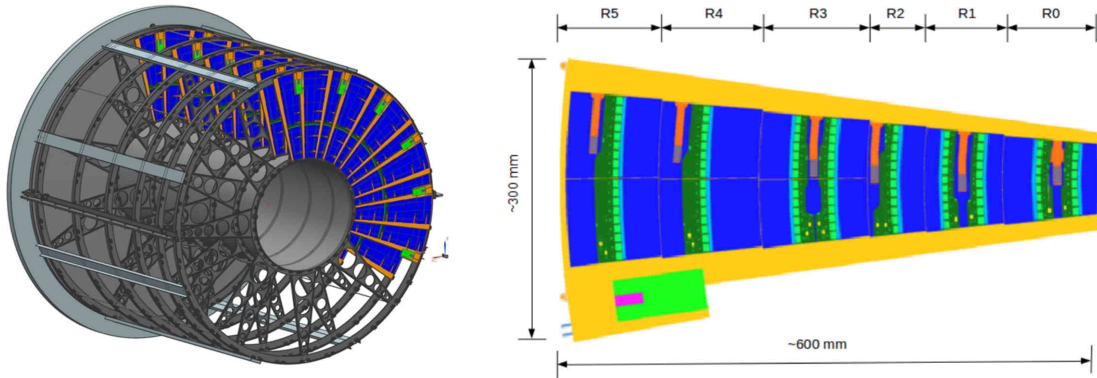

Figure 2.1: ATLAS strip detector end-cap showing petal structures (left) and
design of the petal showing the 6 different modules (right). The module
names R[X] stands for "Ring [X]".

The 6 petal modules are named R0 (closest to the beamline in the radial direction), R1, R2, R3, R4 and R5 . Each module contains, in general, the following components:

⋄ Blank Si, laser cut (320 μm thick).

⋄ FR4 PCBs (200 μm thick).

⋄ Glass ASICs with heater pattern and bonding pads, glued with UV glue, wire-bonded to bare silicon.

⋄ Real DC-DC converters, based on commercial LTC360 ASIC on a custom board.

249   ⋄ Potentiometer to adjust power input/output.

250   − Powered through bus tape power lines.

251   ⋄ In the case of R0 module: v0 assembly tools, real hybrids, glass ASICs.

252   In addition, the prototype counts with real cores (bus tape, honeycomb, Ti V-shaped cooling pipe), real
253 copper power traces, dummy data-lines, and a dummy EoS (not present initially but recently installed)
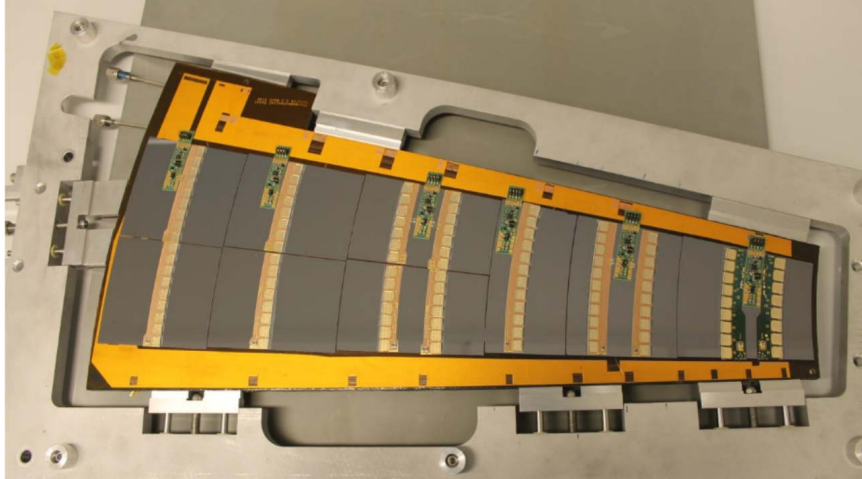254 per side (Figure 2.2).

Figure 2.2: Thermomechanical prototype of the Petal used in the IR
measurements.

255   2.2   Custom Thermal Chamber.

256 For the infrared measurements, the thermomechanical petal prototype was placed inside a customised
257 thermal chamber where, on one end, the petal is installed in its support (Figure 2.3 left) and on the
258 opposite end the IR camera is mounted on a mobile platform that can move horizontally and vertically
259 thanks to an Arduino controlled Gantry System (Figure 2.3 right). Temperature and relative humidity
260 (RH) inside the chamber are monitored using three SHT21 sensors connected to a Raspberry Pi.
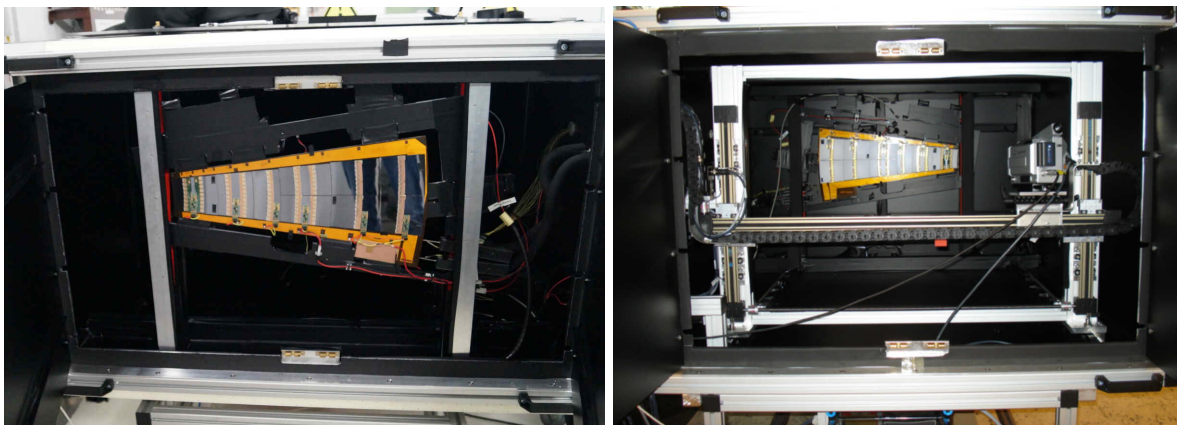

Figure 2.3: Image of both ends of the thermal chamber showing the Petal
already in place and the IR camera also in position.

261   The use of the chamber has two main advantages: on one hand, it provides shielding for the object
262 under investigation against external heat sources such as ceiling lamps, computers and other electronic
263 devices used in the setup; on the other hand, it is used as an enclosure where we can flush nitrogen in

order to reduce the moisture and in doing so preventing condensation from ambient air on the cooled sensors, which would irreversibly damage the prototype. Low RH comes with the additional bonus of reducing the potential absorption of IR radiation in the air path from the target to the IR camera as discussed in Section 1.1. In order to perform the IR measurements and avoid registering the heat from the camera that is reflected back by the petal surface[1], the IR camera is positioned in the chamber in such a way that it faces the Petal with an angle (Figure 2.4).
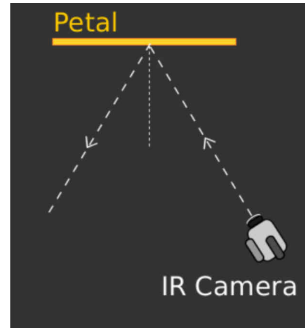

Figure 2.4: The IR camera is placed at some angle with respect to the plane of the petal to avoid the Narcissus effect.

2.3 IR camera.

For this study a VarioCAM High Resolution (hr) IR camera from InfraTec GmbH was used (Figure 2.5). The VarioCAM ® hr is a thermographic system for the long wave infrared spectral range of 7.5 μm to 14 μm (LWIR). The lens images the object scene onto a microbolometer array at a resolution of 640 x 480 pixels. The electrical signal of the detector arrays is further processed by the internal electronics which basically consists in transforming the modified pixel resistance due to the incoming radiation into temperature. The electronics also contains all the functions necessary for camera operation, such as activation of the microbolometer array, A/D conversion, offset and gain correction, defective pixel treatment, video and PC interfaces [8].

The camera's accuracy for temperature measurement (reported by manufacturer) is $\pm 1.5 K$ in the range from 0 °C to 100 °C and $\pm 2\%$ anywhere outside that range. Some additional technical data is presented in Table 2.1.

The data acquisition is performed using the VarioCam hr control software IRBIS ® professional v3.1 (Figure 2.6). Each image is computed as an average of 100 acquisitions regularly taken during five seconds in order to reduce uncertainty due to pixels noise. All thermograms are recorded in units of absolute temperature (K) and emissive power (W/m^2) for further offline analysis.

2.4 Setup configuration.

In this study, two thermal cycles performed using the setup described below are considered, corresponding to both sides of the Petal and measured with the latest experimental configuration. In the following, this will be referred to as "cycle 2" (unpolished side) and "cycle 9" (polished side) in allusion to the dates in which the measurements began (August 2nd and August 9th, 2017).

Much of the improvements of the experimental setup came from experiences of preliminary tests when we realized that, for example, the heat from the Gantry system was being reflected on the Petal's surface and registered by the IR camera. Thus, a curtain from an opaque black fabric was placed between the Petal and the Gantry system (leaving a small hole for the camera lens) to suppress this effect (Figure 2.7 right). In addition, other improvements to the chamber's insulation were made to better control the ambient conditions inside at lower temperatures (Figure 2.7 left).

---

[1]This is known as Narcissus effect and it is an important source of background for the IR measurements if it's not properly handled.

Figure 2.5: VarioCAM ® hr (640 x 480 pixels) IR camera from InfraTec © GmbH.

Table 2.1: VArioCam hr technical data.

|	
Temperature measuring range	(-40 ... 1.200) °C, optional > 2.000 °C
Temperature resolution @ 30 °C	better than 0.08 K, up to 0.05 K (premium mode)
Emissivity	Adjustable from 0.1 to 1.0, in increments of 0.01
Detector	uncooled microbolometer Focal Plane Array
A/D conversion	16 bit
Operation temperature	(-15 ... 50) °C
Humidity during operation and storage	5% to 95%, non-condensing
Shock resistance	25 G, IEC 68-2-29
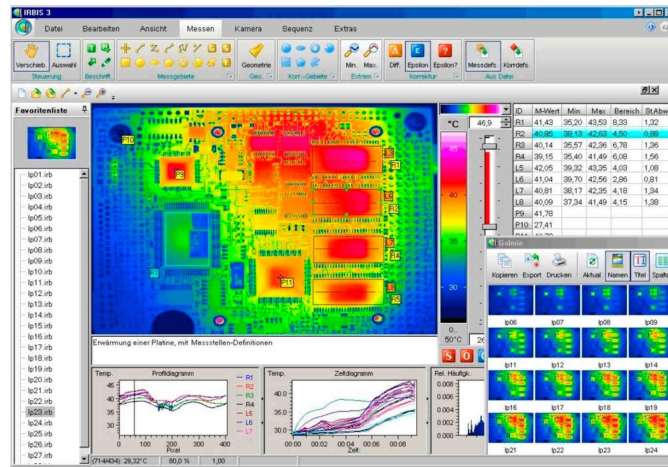
Figure 2.6: Screenshot of the camera's control software IRBIS ® 3.1.

This is particularly important for an accurate estimation of the apparent reflected temperature (See Section 3.1). In addition, the DC-DC converters in modules R2 and R3 were covered with 3D-printed caps and black tape due to the fact that their heat created a "halo" of hot air (Figure 2.8 right) around them that strongly interfered with the IR measurements of that area of the Petal (Figure 2.8 left).

For cooling the Petal the *Transportable Refrigeration Apparatus for CO_2 Investigation* (TRACI) Version 2 (100W) with Lewa pump was used (Figure 2.7 left). This was the first time that we used CO_2 cooling in our set up. Previously, a water-glycol chiller was used, which greatly limited the lowest temperature that we were able to reach.

By controlling the CO_2 pressure in the experiment we were able to adjust the desired temperature working point. Using this method temperatures of near -25 °C were reached.

The petal is equipped with four dummy circuits simulating the heat emitted by the readout electronics (2 Module Electronics + 2 EoS). An important aspect for the prototype operation is that the modules in each side of the petal should have a constant power consumption ($\sim 24W$). The EoS should dissipate
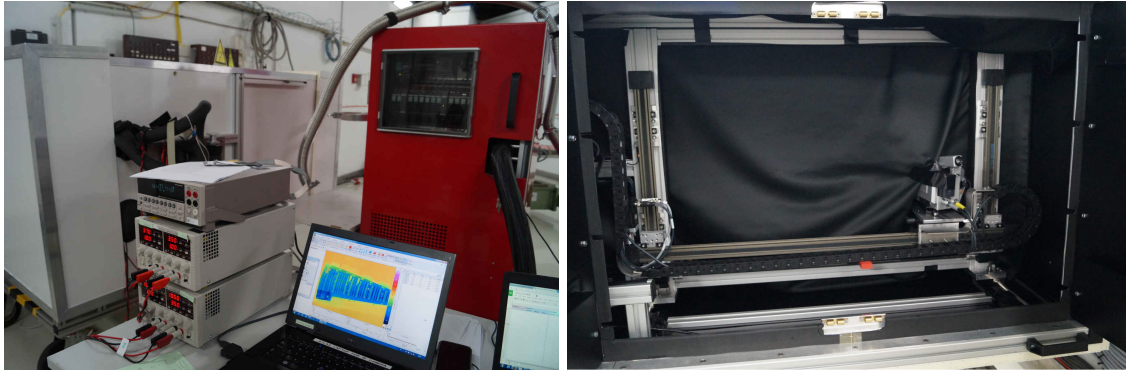
Figure 2.7: Experimental setup used for the Petal's thermal cycles. Right: a view of the chamber with new insulation, laptop for data acquisition, power supplies and Keithley (next to the laptop) and TRACI (Red box). Left: black curtain installation.
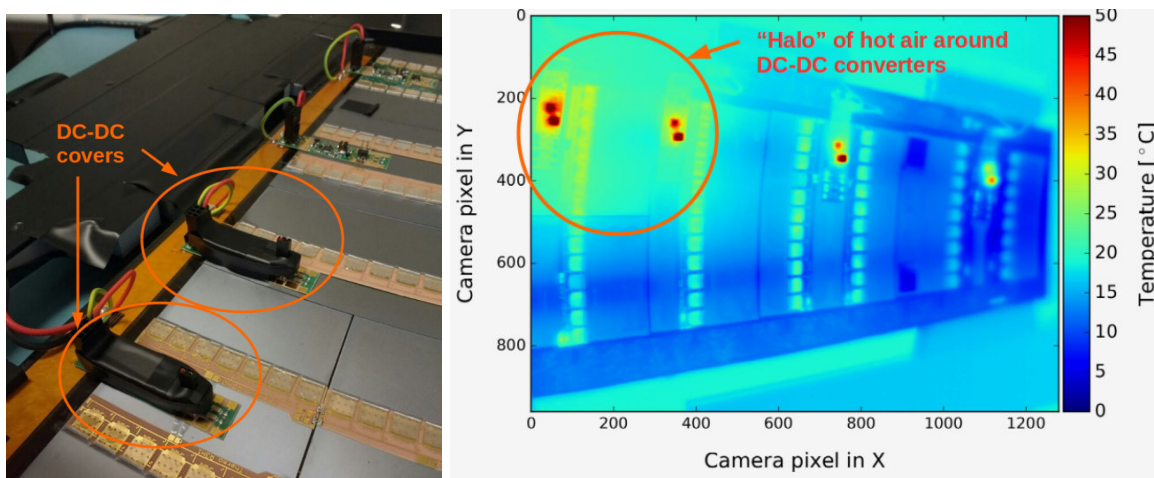

Figure 2.8: Unpolished side of the Petal showing the DC-DC covers (left) and the thermogram where that "halo" of hot air around them is visible inside the circle (right).

3W. To power each side of the Petal and both EoS two TTICPX400 power supply units were used. The modules voltage is set to 10.5V and the current to 2.5A. In the case of the EoS the current is set to 1.0A (for both sides) and the voltage to 3V. However, as the resistance of the circuit changes with temperature we had to vary the voltage accordingly to keep the 3W of power consumption constant. For cycle 2 we did it manually but for cycle 9, as part of the Summer Student program, the student involved in the IR project was able to automatize the process by creating a program that automatically varied the voltage input to keep a steady 3W power consumption [9].

In addition, a Keithley 2700 multimeter was used to register the readings from additional PT100 thermocouples using 4 wire sensing and some other important TRACI parameters like, for example, CO_2 flow, CO_2 temperature before experiment (petal), CO_2 temperature after experiment, pressure setpoint and pressure of the CO_2 in the experiment. Especially, for safety measures, the difference between the pressure setpoint and the pressure in the experiment was maintained around 10 bar.

The additional thermocouples were placed as follows (for cycle 2): 2 on the inlet/outlet pipes (glued), 2 in R3 module silicon surface (not glued): 1 between the ASICs and 1 in the corner next to R4 (Figure 2.9 top). For cycle 9 four extra thermocouples were placed in R0, R1, R4 and R5 as shown in Figure 2.9 (bottom).
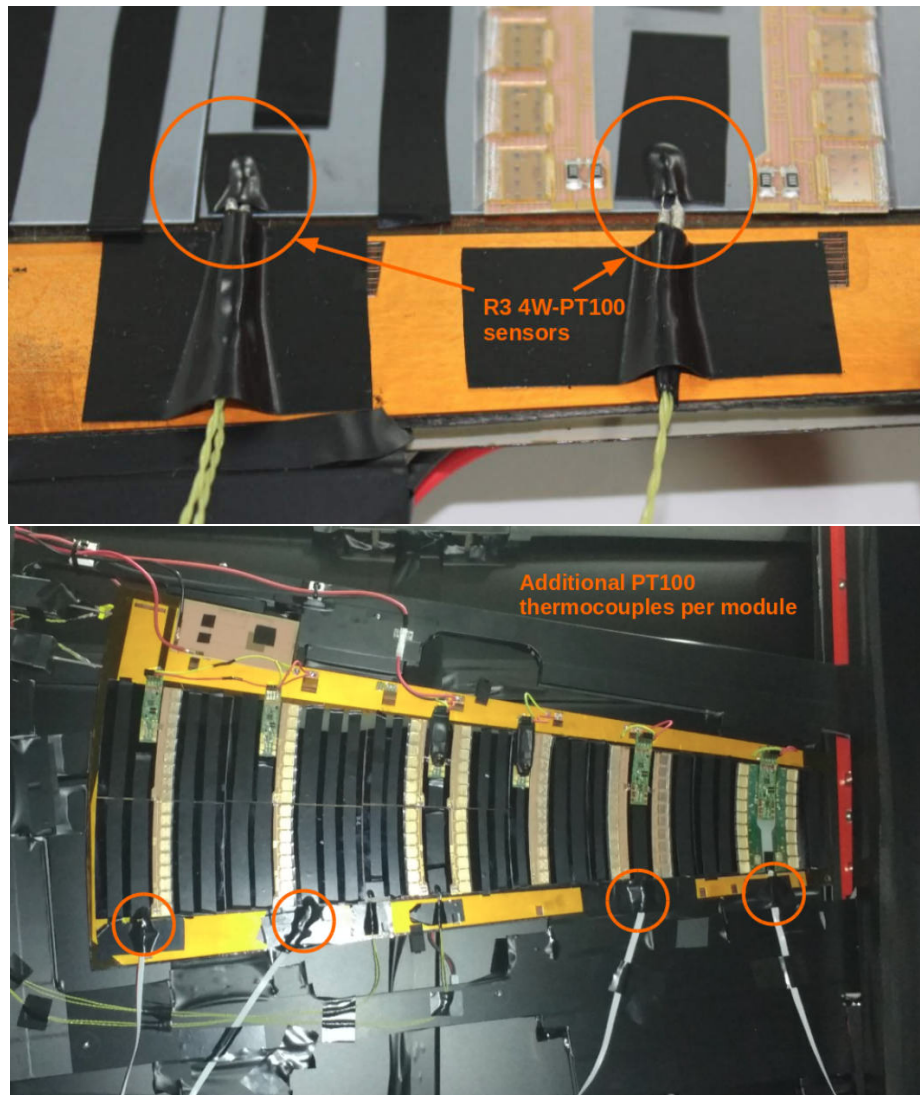
Figure 2.9: Close-up of the unpolished side of the Petal showing the 2 PT100 thermocouples attached to R3 module (top). Polished side of the Petal ready for the thermal test. The additional PT100 thermocouples placed at each module (except R2) are visible (bottom).

Chapter 3

Infrared thermograms analysis

3.1 Apparent reflected temperature estimation.

In order to correctly estimate the emissivity of any surface it is very important to determine first the surface apparent reflected temperature. This is crucial, especially for low emissivity materials where a significant contribution is in fact the reflected radiation.

A simple method can be used to determine the apparent reflected temperature. This method is described as follows:

1) Place a piece of crumpled and re-flattened aluminium foil in the same position of the object to be measured.

2) Set the IR camera emissivity control to 1.00 and distance to 0 m.

3) Point the IR camera to the target and select a region of interest (ROI).

4) Read the value from IR camera on the ROI.

5) Take the measured value as the apparent reflected temperature.

Aluminum foil has very low emissivity ($\sim$0.04) and therefore we are certain that almost all IR radiation coming from the surface is reflected from other sources. The emissivity and distances settings of 1.00 and 0 m respectively are just telling the camera that record everything without applying any further correction. The crumpling is done to allow reflections from several directions, for this reason the ROI selected should be as wide as possible since this effect must be averaged out to obtain an accurate estimate of the apparent reflected temperature.

3.2 IR camera spectral response.

From Equation 1.16 it can be seen that if we can accurately estimate emissivity, apparent reflected temperature and the IR camera spectral response function (R) we should be able then to obtain the real temperature of the object for any given spectral power value reported by the camera (N_{meas}).

In order to estimate the R factor we can simply take the emissive power measurements of a surface of known emissivity, the real temperature and the apparent reflected temperature and then use the same Equation 1.16 to derive the R scale factor. As this factor only depends on the IR camera, it can be used later on in the analysis as long as we don't use a different camera. For obtaining the scale factor we used an aluminum bucket which we filled with hot water and recorded the IR power density on several points of the surface (always at the same depth) coated with black tape as the water temperature went down to test the temperature independence of the results (Figure 3.1).

With this scale factor and Equation 1.16 we could estimate emissivity at pixel level if we had a thermogram in which the real temperature of all the pixels is known. In the next section we will refer to this method as the "baseline image" method.
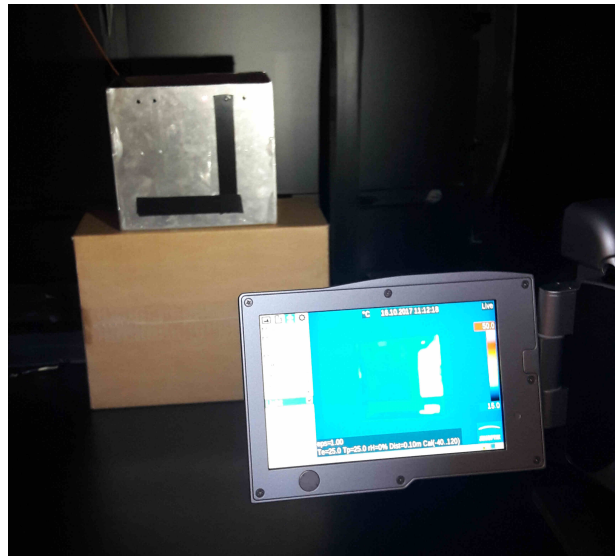
Figure 3.1: Experimental setup to calculate the IR camera spectral response function. Measurements were performed placing height measurement markers along the horizontal black tape in the camera IRBIS software.

3.3   Emissivity estimation.

As the main source of discrepancies comes from the differences in emissivity, this is very often the starting point for IR image calibration. Almost all IR cameras can be set to a certain value of emissivity (usually set to one by default). If we knew the emissivity value of certain surface we could then enter that value into the IR camera software and the apparent temperature, i.e. temperature displayed by the IR camera, would be close to the real temperature. This is what we would call a "direct" emissivity correction method. It is of course the most simple but also the most uncommon way to correct an IR image for more complicated quantitative studies. On one side, we usually don't know beforehand the emissivity value of the surface we want to measure and, on the other side, this method would only give us the correct temperature on the surface of known emissivity.

There are also some other ways to calculate the emissivity of a surface. One of them consists in estimating the surface's emissivity by using an alternative temperature measurement as reference. With that purpose, the following method can be used [10], [11]:

1) Measure the surface temperature by an alternative method (thermocouple, known emissivity coating).

2) Set the necessary measurement parameters in the IR camera software and the emissivity to 1.

3) Point the IR camera to the target and select a region of interest (ROI).

4) Modify the value of emissivity in the camera software until the apparent temperature in the selected ROI equals the one measured with the alternative method. This is the emissivity of the target surface.

5) Repeat steps 2) to 4) as many times as necessary to minimize the measurement uncertainty.

Using this approach a "global" IR image emissivity correction can be applied to get temperature values close to the real ones in the silicon surface. However, as mentioned before, this will only show accurate readings in those areas corresponding to the surface of estimated emissivity. The rest of the elements in the image that have different emissivity values might appear to have a complete different temperature of what they actually have. However, if we are not interested in the whole picture but just in one particular material in it, this simple method can be very useful. The problems begin when the surface of interest has relatively low emissivity. In such cases temperature estimation may not be very accurate because low emissivities are hard to estimate and small changes in their values can lead to large variations in the temperature measurements [12]. In other words, the lower the emissivity of the surface, the bigger the uncertainty associated with it [13].

Another approach consists in using a "relative" method exploiting the Equation 1.16. Lets imagine that we have two surfaces at the same temperature, then, if we apply Equation 1.16 on the one that we know the emissivity value (e.g. black tape) and on the one we want to estimate it from (e.g. silicon surface) then we obtain:

$$N_{meas}^{BT}(T_{BT}) = R \cdot \bar{\varepsilon}_{BT} \cdot I_1(T_{BT}) + R \cdot [1 - \bar{\varepsilon}_{BT}] \cdot I_2(T_r) \tag{3.1}$$

$$N_{meas}^{Si}(T_{BT}) = R \cdot \bar{\varepsilon}_{Si} \cdot I_1(T_{BT}) + R \cdot [1 - \bar{\varepsilon}_{Si}] \cdot I_2(T_r) \tag{3.2}$$

Here T_{BT} is the apparent (measured with the IR camera) temperatures of the black tape. Note that as the "real" temperature we have selected the apparent temperature of the black tape. We can do so since the black tape has high emissivity. Naturally we know that $N_{meas}^{BT}(T_{BT}) \neq N_{meas}^{Si}(T_{BT})$, however, we can use a small trick here: as the black tape has high emissivity, if we replace T_{BT} in Equation 3.1 with the apparent temperature of the silicon (T_{Si}) then $N_{meas}^{BT}(T_{Si}) = N_{meas}^{Si}(T_{BT})$ and after rearranging terms we obtain:

$$\bar{\varepsilon}_{Si} = \bar{\varepsilon}_{BT} \cdot \frac{I_1(T_{Si}) - I_2(T_r)}{I_1(T_{BT}) - I_2(T_r)} \tag{3.3}$$

Note that this expression is invalid if the silicon surface is considerably transmissive, since we have neglected transmissivity for deriving Equation 1.16, and when the real temperature (T_{BT}) is close to T_r in which case Equation 3.3 does not hold anymore. This is known as the "black tape method" and, as the name indicates, consists in covering the surface of interest with a material of known emissivity (usually high emissivity) and use the direct correction method on the coated surface.

For the Petal's thermal study, parts of the silicon surface on both sides were covered with high emissivity black tape (Figure 3.2). The black tape used has an emissivity of 95% and therefore the coated surface will behave almost like a blackbody.
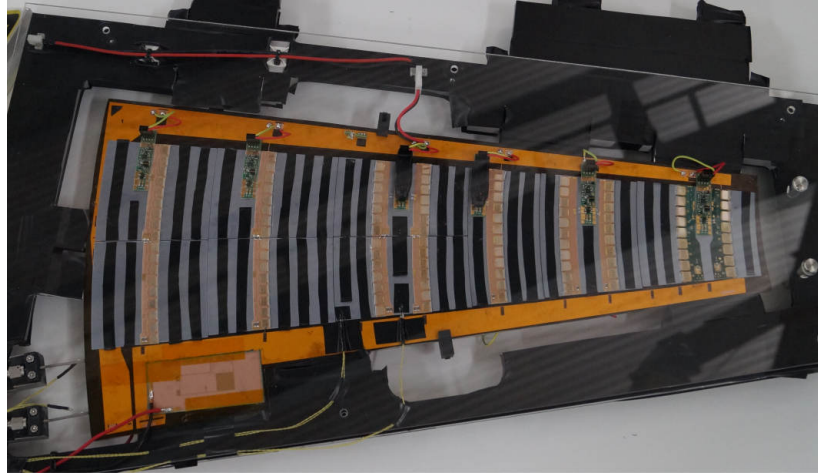

Figure 3.2: Unpolished side of the "Zebra" Petal covered with stripes of black electrical tape of high emissivity.

For our black taped petal ("zebra"), setting the IR camera emissivity to the emissivity of the black tape we can measure an apparent temperature very close to the real temperature assuming that both the surface of interest and the black tape on top of it have reached a steady state at the same temperature. Using the IRBIS software a set of over 560 measurement markers (ROIs) were created on the black tape strips to create a map of trustable temperatures. With this method we could perform calibrated temperature measurements on the Petal's silicon surface to be able to compare with FEA simulations (See Chapter 4). However, as it can be seen from the picture, we had to add adhesive material onto the silicon surface, which would be unacceptable during production stages for quality control. Additionally, a set of markers was created on the silicon surface right next to the corresponding black tape marker

to be able to estimate the emissivity of the silicon using the black tape markers readings as the "real" temperature values.

Let's now discuss another method, known as the "baseline image" method. If we assume that we have a thermogram of which we know the real temperature of all the pixels. That could be, for example, a thermogram of the Petal at room temperature (Figure 3.3). The fact that we still see differences of temperature in the image even though everything is at the same temperature is evidence (to a first approximation) of the effect of the different emissivity values of the materials composing the Petal. We call such image a baseline thermogram. The advantage of the *baseline thermogram* is that we know the real temperature of all the pixels beforehand and therefore we could use Equation 1.16 to calculate the emissivity of each pixel.
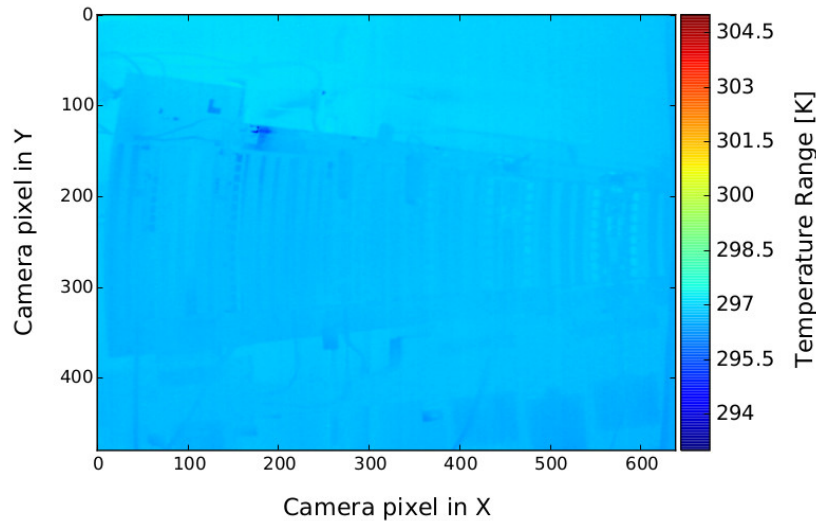

Figure 3.3: Thermogram of the petal at room temperature (not powered and no CO2 flushed in). Even though everything is at the same temperature, we still can see the shape of the petal.

This method, however, presents an associated difficulty: if the baseline is at room temperature, it means that we can not use Equation 1.16 directly to obtain emissivity but, instead, we can use it iteratively to estimate emissivity to some degree of accuracy. Of course this makes even worse the errors in the estimation of emissivity but it's the price to pay for not touching the petal. The other important disadvantage is that, in order to be able to extrapolate the values of emissivity calculated on the baseline image to other thermograms we must be sure that the camera does not move from one to the other, otherwise the pixels won't match anymore and the emissivity values would not be valid.

Finally, we have also assumed that the emissivity does not depend on the surface temperature under the graybody approximation, which is not true in general. However, except for the case of selective emitters, emissivity is a very slowly-variating function of the surface's temperature.

3.4   Viewing angle influence.

In order to determine whether the viewing angle of the camera with respect to the normal to the petal surface is a determining factor in our analysis, an angular study was performed using an aluminum rod filled with hot water placed in the same position as the Petal. and, using a strip of high emissivity black tape along the rod's frontal face we were able to measure the variations in temperature due to the viewing angle (Figure 3.4).

Figure 3.4: Aluminum rod used to study the angular dependence of emissivity

A set of measuring areas (ROI) was defined along the rod using the IR camera software (IRBIS) and a thermocouple was inserted inside the rod in direct contact with the water in order to be able to determine the real temperature of the ro's surface.

Chapter 4

Results and discussion

4.1 Petal thermal cycles.

For both thermal cycles the set points were selected by varying the CO_2 pressure in such a way that we go from room temperature to the lowest possible temperature and back to room temperature in steps of 5 °C. Then, at each set point, the following data is recorded:

1) Inlet/outlet pipes temperatures (PT100).

2) Temperature readings (PT100) on the silicon surface at each module (See Figure 2.9).

3) CO_2 flow.

4) Temperature of the CO_2 going in/out of the petal.

5) Pressure of the CO_2 going into the petal and the difference to the pressure setpoint.

6) Ambient temperature and RH inside the chamber.

7) Voltage/current readings from the power supply units.

Also, the Petal thermograms are recorded following the method described in Section 2.3 at each step. The results are shown in Figure 4.1 for both cycles 2 and 9. Uncertainties of the IR measurements have not been included not to overload the plots but, as discussed also in Section 2.3, the main source of uncertainty comes from the IR camera itself.

As it can be seen, with cycle 2 (cycle 9) we were able to reach temperatures of around -18 °C (-20 °C). For both cycles it is also notable that the returning CO_2 is colder, which is consistent with dual-phase cooling. We can also see that the PT100 thermocouple sensors report consistently higher temperatures that the TRACI sensors for both inlet and outlet pipes. Either we lost some cooling power due to thermal conductivity of the pipes, which is expected, or one of the sensors got incorrectly calibrated/placed. This situation is the opposite in cycle 9 with the inlet fluid temperature readings. In fact, for cycle 9, the inlet PT100 accidentally broke and had to be reglued which might explain the difference from one cycle to the other in the inlet pipe while the outlet remained somewhat the same. This indicates that a correct manipulation of the thermocouple sensors is crucial to obtain good reliability on the measurements.

Another interesting test that we wanted to perform was the comparison between the temperature reported by the IR camera using the black tape method and the temperature measured with an alternative method on the same surface (e.g. using PT100 thermocouples). In order to perform such a test, the additional PT100 sensors placed on the silicon surface were hold in position using the same high emissivity black tape used for the strips of the "Zebra" Petal. For cycle 2 only two PT100s were used, as described in Section 2.4 while for cycle 9 four additional ones were placed. From Figure 4.1 (top) we can see that the readings of the thermocouple and the IR camera are quite different for the sensor placed between the ASICs, possibly due to miss-contact with the silicon surface (the sensors had to be placed very carefully not to damage the silicon). The other PT100 sensor, on the other hand, shows relatively good agreement with the IR camera measurement. The situation in cycle 9 improved a bit more, in general, for the lowest setpoint, specially in the R0, R3(border) and R4, even though there are still large discrepancies (e.g. R5). With this results we also see that the tendency of the sensors is to not having memory (i.e. they are not damaged) after the thermal cycles, which was one of the main concerns that motivated the thermal tests.
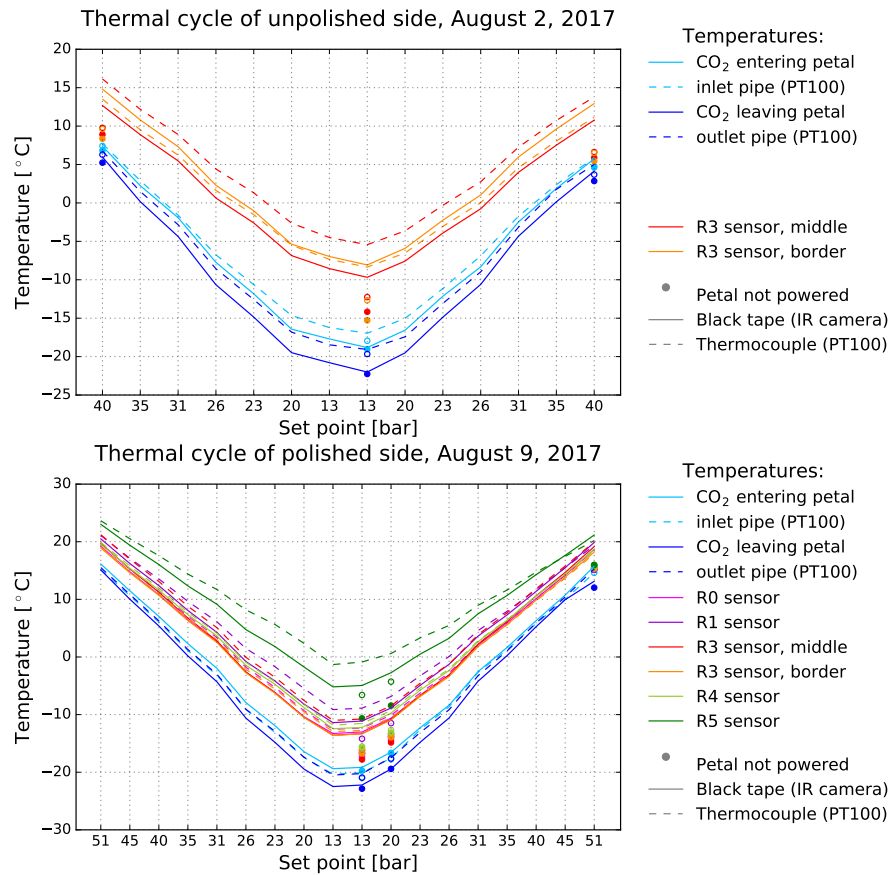
Figure 4.1: Temperature plots for the thermal cycles corresponding to the polished (front) and unpolished (back) sides. The dots represent set points with the Petal not powered and the lines correspond to set points with both sides of the petal powered. Solid lines and filled dots represent black tape readings with the IR camera (except CO_2 entering/leaving petal) and dashed lines and hollow dots represent thermocouple values.

4.2   Comparison with FEA results.

In order to compare the results with FEA simulations, the IR camera temperature measurements from ROI markers on the surface of the black tape strips was used. Figure 4.2 shows the lowest point thermogram for cycle 2 where the tiny red squares are the IRBIS measurement markers. Using linear interpolation between the marker points we were able to produce an isotherm map of the sensors as shown in figure 4.3(top). Figure 4.3 (bottom) shows the corresponding FEA simulation results [14].

Before discussing the differences between the images in Figure 4.3, we must say that this is to some extent an unfair comparison. While in FEA one have access to virtually every temperature point we are limited here by the number of markers and their uncertainty. Furthermore, the characteristics of the FEA model are not exactly compatible (e.g. power board thickness, cooling loop) and the very complicated convection/absorption with the air surrounding the Petal is very hard to model. In fact, we know that the values of temperature reported by the markers near the R3 electronics (hottest point) is greatly influenced by the "halo" surrounding it, as discussed in Section 2.4. In addition, in that precise region of the image, the linear interpolation tries to figure out a large area where there is no experimental point and thus, this area should not be very well described.

In general (without paying too much attention to the temperature magnitudes), some similar features can be found between the experimental results and the FEA model, specially to the left side of the Petal (R4 and R5).
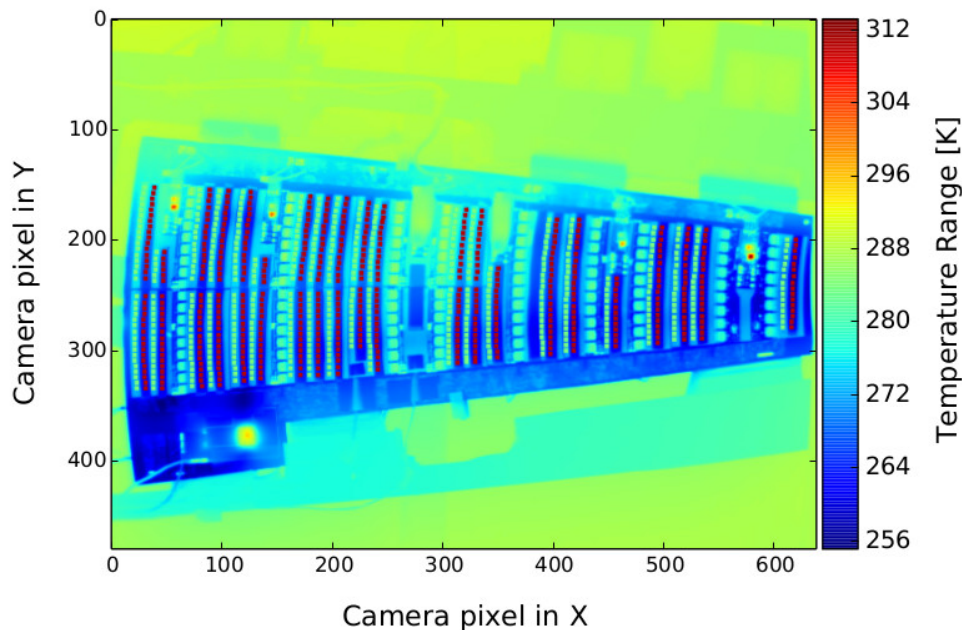
Figure 4.2: Thermogram of the lowest setpoint in cycle 2 showing the IRBIS
measurement areas (markers) defined on the black tape (red squares) and the
corresponding silicon surface ones (blue squares).

4.3   Silicon emissivity estimation.

As shown in the previous section, one of the factors affecting the robustness of the measurements is the lack of "resolution" by using the black tape method, even though more than 560 markers were created (by hand) on the surface of the silicon sensors. This asks for more refined ways to measure the temperature of the silicon sensors. Furthermore, the black tape method is a quite invasive technique to use with the current prototype and for sure something to avoid during quality control with real Petals.

A good first approach would be to try to estimate the silicon emissivity and then use this value to correct globally the IR image. As mentioned in Section 3.3, a "relative" method using the black tape markers measurements as temperature reference can be used to calculate the emissivity of the silicon next to them employing Equation 3.3. The IRBIS software also has an emissivity calculator which reports the emissivity of a given pixel if we provide the real temperature of the pixel and the ambient temperature (apparent reflected temperature). However, as this variant is more like a black box to us, we decided to use both methods and compare the results. As mentioned also in Section 3.3, Equation 3.3 will only work for opaque surfaces (not transmissive) and for surface temperatures well away from the apparent reflected temperature. For those reasons we performed this study on the unpolished side of the Petal since the polished side is highly transmissive (Figure 4.4).

Figure 4.5 shows a profile plot of one of the black tape strips in sensor R3 at the lowest setpoint. We can see how both silicon and black tape markers readings show two minima corresponding to the position through which the cooling pipe goes underneath the surface. It is appreciable the difference between the temperature values of black tape and silicon markers. This is mainly due to differences in emissivity: since the silicon surface has lower emissivity than black tape, the apparent temperature is higher. This apparent contradiction can be overcome if we think about it this way: since the black tape has higher emissivity, it is therefore better than the silicon at emitting the real (cold) temperature.

After applying Equation 3.3 on each pair of silicon - black tape markers and using the IRBIS software emissivity calculation tool we obtained the results shown in Figure 4.6. As we can see the Equation 3.3 estimations are in good agreement with the software outputs.

The average emissivity is estimated to be around 0.66 ± 0.07. By entering this value in the IRBIS software we could correct "globally" the pixels temperature to yield silicon temperatures more close to the real values. However, this would worsen the calibration for the rest of the surfaces making their temperature values to shift greatly from the truth value.
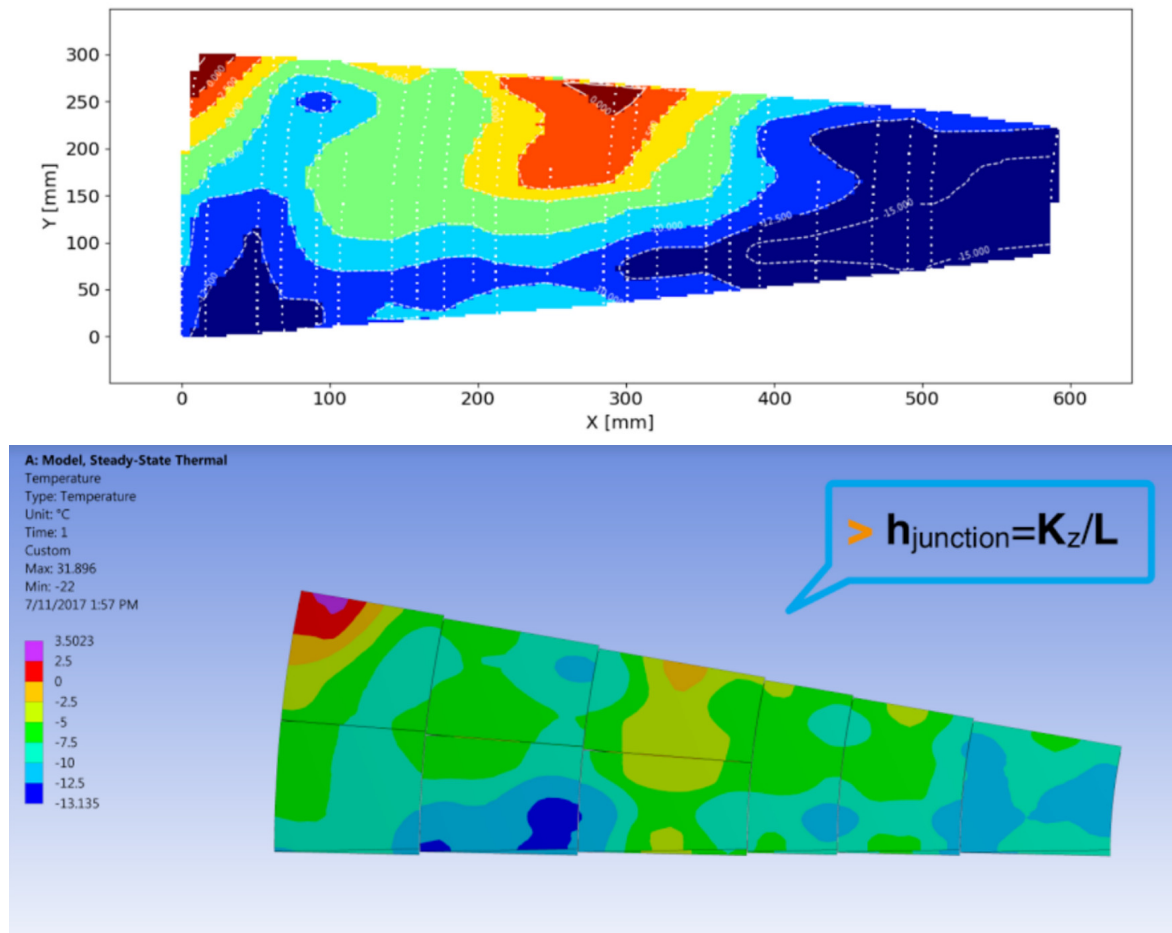
Figure 4.3: Temperature profiles for the silicon sensors of the unpolished side of the Petal. (Top): experimental IR measurements results. (Bottom): FEA simulation.

Figure 4.4: IR image (taken directly with the camera) of a circular piece of silicon wafer similar to the one glued on the polished side of the Petal showing the high transmissivity properties of the silicon. Behind the silicon there is a heating plate at 150 $^\circ C$ and in between the experimenter's hand (we can clearly see the fingers shape through the silicon).
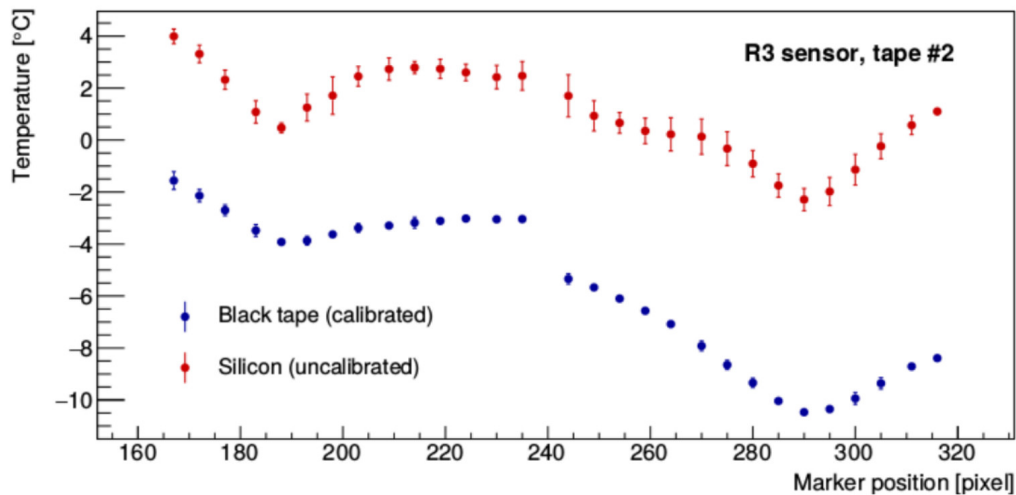
Figure 4.5: Temperature profile plot of the second (middle) black tape strip in module R3 for the lowest temperature setpoint.
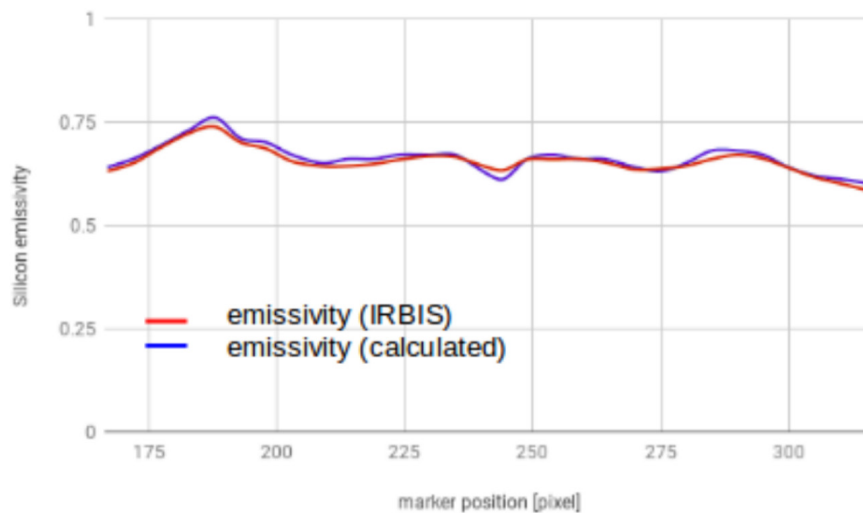

Figure 4.6: Silicon emissivity calculated using Equation 3.3 (blue line) and the emissivity calculation tool provided by the IR camera software (red line).

4.4 IR camera spectral response scale factor.

Figure 4.7 (left) shows the results of the estimation of the R scale factor for the IR camera. The method used was described in Section 3.2, however, to test the method's validity we used as well a Petal thermogram of which we knew the real surface temperatures, that is, the powered off Petal at room temperature. Figure 4.7 (right) shows the scale factor estimation on the Petal.

For the calculations, the values of the black tape in silicon modules R0, R1 and R2 were used, showing consistent results with the values obtained with the aluminum bucket. The uncertainty shown is the fit's root mean squared error. With this test we corroborated that this factor is only dependent on the IR sensor/camera and independent of the temperature and the surface.

4.5 Viewing angle influence in the measurements.

In order to test whether or not the viewing angle played a significant role in the IR temperature measurements, the aluminum rod described in Section 3.4 was used, filled with water at 34.6 °C. The results can be seen in Figure 4.8.
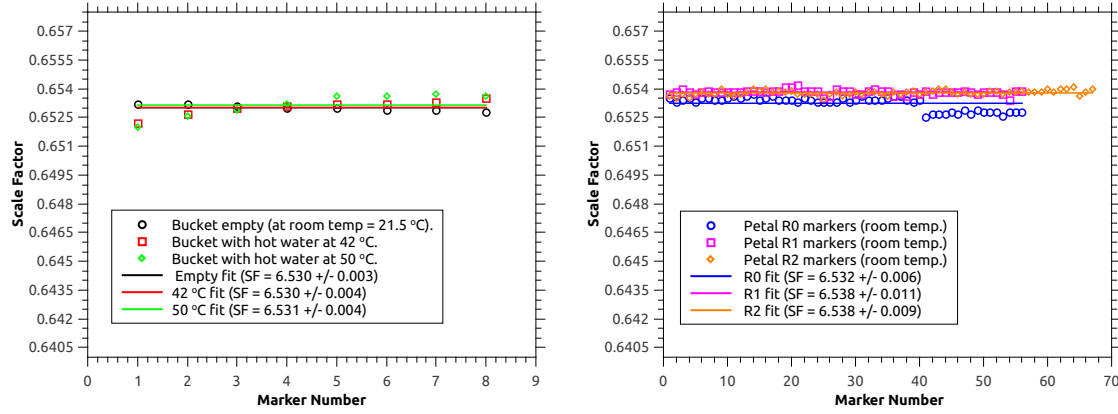
Figure 4.7: Fits of the IR camera response scale factor calculated for different temperatures (left) and using a Petal thermogram (right).

We observed that the temperature variations along the rod are within $1 \ ^\circ C$ including the error bands from an angle of $0°$ (with respect to the normal of the rod's surface) to roughly $30°$. For the central values this difference is less than $0.2 \ ^\circ C$. This is a relatively small variation for that angular range and even though we see a drop in the markers temperature with respect to the real temperature (measured with a thermocouple directly inside the rod) the error magnitude make us conclude that, within this uncertainty, the angle influence on the IR temperature measurements is quite negligible.
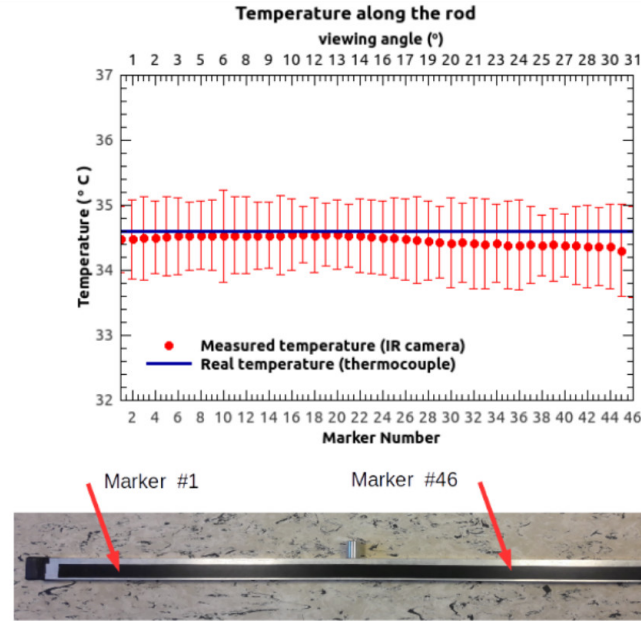

Figure 4.8: Angle study results (top) using the aluminum rod filled with water at 34.6 $^\circ C$ (bottom). The marker positions do not cover the entire rod since it is larger than the Petal and some portions fall out of the viewing field of the camera.

CONCLUSIONS

The results of the last two thermal cycles performed on the thermomechanical prototype of the petal are presented. For the first time, a CO_2 cooling system was used, which allowed us to reach lower temperatures (about -20 $°C$ at inlet pipe). Also, some improvements in the experimental setup related to the insolation of the thermal chamber and data acquisition procedure were adopted. Several PT100 thermocouple sensors were placed on the petal's silicon surface to obtain an alternative temperature reading to compare with the IR measurements. In general, the thermocouples readings and the camera ones (corrected using the black tape method) behave quite similar for most of the sensors. Discrepancies arise possibly related to misplacement of the PT100s are observed for a couple of sensors.

Using a set of over 560 measurement areas defined in the IRBIS software, a temperature map of the petal modules was obtained using linear interpolation. The results were compared with the results obtained with the FEA model showing promising similarities.

Emissivity of the silicon surface of the unpolished side of the petal has been estimated to be $\varepsilon = 0.66 \pm 0.07$, assuming no transmissivity, which is in good agreement with the values calculated using the emissivity calculation tool provided by the IR camera software. For the polished side we expect the value to be much less since the surface is highly reflective. This method allows us to globally correct the petal thermograms to show more realistic temperature values (only) on the surface of the silicon.

In addition, the IR camera spectral response scale factor was calculated using an alternative setup consisting in an aluminum bucket filled with water. The results were compared with the ones obtained using a petal thermogram (not powered at room temperature) showing good agreement, as expected for a magnitude only dependent of the IR sensor.

Finally, it is shown how the camera's viewing angle has no appreciable influence in the temperature measurements with this particular experimental setup.

REFERENCES

[1] ATLAS Collaboration, "Technical Design Report for the ATLAS Inner Tracker Strip Detector", Tech. Rep. CERN-LHCC-2017-005. ATLAS-TDR-025, CERN, Geneva, Apr 2017.

[2] C. Meola, *Infrared Thermography Recent Advances and Future Trends.* Bentham Science, New York, 2012.

[3] J. R. Howell and R. Siegel, *Thermal Radiation Heat Transfer.* Hemisphere Publishing Co., third ed., 1992.

[4] R. Usamentiaga et al., "Infrared Thermography for Temperature Measurement and Non-Destructive Testing.", *Sensors*, vol. 14, pp. 12305-12348, 2014.

[5] S. Chomet and G. Gaussorgues, *Infrared Thermography.* Chapman and Hall, first ed., 1994.

[6] K. Moellmann et al., "Selected critical applications for thermography: Convections in fluids, selective emitters and highly reflecting materials.", *In Proceedings of the Infrared Camera Calibration Conference*, vol. 6, (Las Vegas (NV), USA), pp. 161-173, oct 2015.

[7] M. Vollmer and K.-P. Moellmann, *Infrared Thermal Imaging: Fundamentals, Research and Applications.* Boschstr. 12, 69469 Weinheim, Germany: Wiley-VCH Verlag GmbH, 2010.

[8] InfraTec GmbH, Gostritzer Strasse 61-63, *VarioCAM ® high resolution user manual*, nov 2015.

[9] [reference to maximiliam's report]

[10] ASTM E1933-97. "Standard Test Methods for Measuring and Compensating for Emissivity Using Infrared Imaging Radiometers", 1997.

[11] ISO 18434-1:2008. "Condition monitoring and diagnostics of machines–Thermography– Part 1: General procedures", 2011.

[12] S. Marinetti and P. G. Cesaratto, "Emissivity estimation for accurate quantitative thermography", NDT & E International, vol. 51, pp. 127-134, oct 2012.

[13] B. Sopori et al., "Calculation of emissivity of si wafers", Journal of Eletromagnetic Materials, vol. 28, no. 12, 1999.

[14] [Yu-Heng's report on FEA ...]